*Open*
ORIGINAL ARTICLE

Cell Research (2016) 26:517-528.
www.nature.com/cr

# MLKL forms cation channels

Bingqing Xia[1], Sui Fang[1], Xueqin Chen[1], Hong Hu[2], Peiyuan Chen[1], Huayi Wang[2], Zhaobing Gao[1]

*[1]CAS Key Laboratory of Receptor Research, Shanghai Institute of Materia Medica, Chinese Academy of Sciences, 555 Zuchongzhi Road, Shanghai 201203, China; [2]School of Life Science and Technology, Shanghai Tech University, Shanghai 200031, China*

**The mixed lineage kinase domain-like (MLKL) protein is a key factor in tumor necrosis factor-induced necroptosis. Recent studies on necroptosis execution revealed a commitment role of MLKL in membrane disruption. However, our knowledge of how MLKL functions on membrane remains very limited. Here we demonstrate that MLKL forms cation channels that are permeable preferentially to $Mg^{2+}$ rather than $Ca^{2+}$ in the presence of $Na^{+}$ and $K^{+}$. Moreover, the N-terminal domain containing six helices (H1-H6) is sufficient to form channels. Using the substituted cysteine accessibility method, we further determine that helix H1, H2, H3, H5 and H6 are transmembrane segments, while H4 is located in the cytoplasm. Finally, MLKL-induced membrane depolarization and cell death exhibit a positive correlation to its channel activity. The $Mg^{2+}$-preferred permeability and five transmembrane segment topology distinguish MLKL from previously identified $Mg^{2+}$-permeable channels and thus establish MLKL as a novel class of cation channels.**

***Keywords*:** MLKL; magnesium channel; bilayer lipid membrane; cation channel; necroptosis
*Cell Research* (2016) **26**:517-528. doi:10.1038/cr.2016.26; published online 1 April 2016

## Introduction

Necroptosis is a type of programmed necrosis involved in development, immune response to viral infection, and inflammatory injury [1, 2]. It was first observed in certain cell types after the treatment of tumor necrosis factor (TNF), a cytokine that also induces NF-κB activation and apoptosis [3-5]. Although necroptosis has been best described as a TNF-induced cellular response, it can also be induced by various other stimuli, such as Fas ligand, interferon, lipopolysaccharides, and viral DNA/RNA [6-12]. After necroptosis induction, two kinases, receptor-interacting protein 1 (RIP1) and RIP3, are sequentially activated, which recruit the mixed lineage kinase domain-like (MLKL) protein to form the necrotic death complex called necrosome. MLKL is phosphorylated at T357/S358 (in human) by RIP3 [13]. Deletion of the *MLKL* gene or an alanine mutation at the phosphorylation site of MLKL prevents necrosis but does not affect necrosome assembly, suggesting that MLKL is the *bona fide* substrate of RIP3 and is specifically required for necrosis signaling [13-18].

Necrosis is characterized by necrotic morphological changes, including organelle swelling and membrane rupture. The general steps from MLKL phosphorylation to cellular membrane damage have been elucidated. RIP3 phosphorylates MLKL at the activation loop of the kinase-like domain, causing MLKL proteins to oligomerize. Biochemical fractionation study using MLKL phospho-antibody has revealed that phosphorylated MLKL is located in cell membrane fractions, suggesting that the MLKL oligomer functions in membranes [13]. MLKL comprises an N-terminal helical bundle domain (referred to HBD), and a C-terminal kinase-like domain [19]. Overexpression of a phosphomimetic mutant of MLKL or a truncated construct lacking the kinase-like domain results in necrosis bypassing RIP3 [19, 20]. Recombinant MLKL proteins containing HBD can cause dose-dependent liposome leakage [21]. There is evidence that MLKL forms permeable large pores that allow the leakage of 10-kDa molecules, thereby disrupting cell membrane integrity and causing cell lysis [13]. However, other studies reported an influx of $Na^{+}$ or $Ca^{2+}$ after the formation of MLKL oligomer, which can potentially contribute to necrosis, suggesting that $Na^{+}$ and/or $Ca^{2+}$ channels function downstream of MLKL [22, 23]. Moreover,

Correspondence: Huayi Wang[a], Zhaobing Gao[b]
[a]E-mail: wanghuayi@shanghaitech.edu.cn
[b]E-mail: zbgao@simm.ac.cn
Received 5 December 2015; revised 1 February 2016; accepted 1 February 2016; published online 1 April 2016

one transient potential receptor (TRP) channel, TRPM7, is suggested to mediate $Ca^{2+}$ influx in necrotic cells [22]. Regardless of the controversy, ion disturbance in necrosis may simply be explained as the consequence of membrane penetration by MLKL. The N-terminal HBD of MLKL is believed to serve as a membrane perforator. The solution structure of the N-terminal part of human MLKL reveals six α-helices, H1 to H6; among them H1, H2, H3, and H5 form the HBD [21]. Interestingly, the architecture of MLKL is not similar to any of the known ion-channels or pore-forming proteins. How MLKL behaves in the membrane remains obscure.

In this study, we provide direct evidence that MLKL forms transmembrane cation channels. The MLKL channel is permeable to $Mg^{2+}$, $Na^+$ and $K^+$ but not $Ca^{2+}$, making it unique among cation channels. The configuration of MLKL HBD in membrane is also described, enriching our knowledge of this new type of cation channel.

## Results

*MLKL mediates typical single-channel currents*

MLKL phosphorylation and oligomerization is sufficient and necessary for its function in necroptosis. The phosphomimetic mutations T357E/S358D ($MLKL^{E/D}$) shift the protein to an oligomeric state, whereas the T357A/S358A mutations ($MLKL^{A/A}$) prevent this transition [13]. To examine the potential currents mediated by MLKL in the membrane, both $MLKL^{E/D}$ and $MLKL^{A/A}$ were purified and examined using a planar lipid bilayer recording technique. Both a large-scale current with amplitude of 30-40 pA and square step-like multiple-channel currents were observed following the addition of purified $MLKL^{E/D}$ into the neutral symmetric 50 mM NaCl solutions (pH = 7.0; Figure 1A). In contrast, the protein $MLKL^{A/A}$ did not elicit current-like signals for 1 h under the identical condition (Figure 1B). Moreover, typical single-channel signals could be induced and characterized over extended periods of time when the concentration of $MLKL^{E/D}$ was reduced (Figure 1C, bottom panel). The average current amplitude of the single-channel currents was 2.8 ± 0.1 pA ($n$ = 10). The open-time distribution can be fitted well by a bi-exponential equation, revealing two time constants (Figure 1D). The above results demonstrate that $MLKL^{E/D}$ forms ion channels.

*MLKL channels are cation selective*

Ion permeability is one of key characteristics that define a class of ion channels. The ability of MLKL channels to distinguish anions and cations was examined (Figure 2A and 2B and Supplementary information, Figure S1). In symmetric 50 mM NaCl solutions, $MLKL^{E/D}$ channels exhibited a linear current-voltage relationship and a reversal potential of 0 mV. Asymmetric 15:150 mM (*cis*:*trans*, *cis* side is where the protein was added) NaCl solutions did not affect the linear current-voltage relationship but left-shifted the reversal potential to −63.7 mV, which is very close to the theoretical equilibrium potential of $Na^+$, indicating that the $MLKL^{E/D}$ channels are permeable to $Na^+$ but not to $Cl^-$. To determine whether the $MLKL^{E/D}$ channel can distinguish $Na^+$ and $K^+$, the two major physiological monovalent cations, the influence of additional $K^+$ on the reversal potential of $Na^+$ was examined. The addition of 150:15 mM (*cis*:*trans*) $K^+$ solutions resulted in a shift of the reversal potential to −6.0 mV from −63.7 mV, indicating that the $MLKL^{E/D}$ channels cannot distinguish $Na^+$ and $K^+$ ($P_{Na}/P_K$ = 1.5). These results demonstrate that MLKL channels are permeable to monovalent ions $Na^+$ and $K^+$ but not to $Cl^-$. Hence, MLKL forms cation-selective channels.

*MLKL forms $Mg^{2+}$-preferred channels*

The permeability of MLKL channels to $Ca^{2+}$ or $Mg^{2+}$, two physiological important divalent cations, was then evaluated in $Na^+$ solutions premixed with either of the two ions. For the $Na^+/Ca^{2+}$ solutions, we found that $MLKL^{E/D}$ did not induce detectable currents, regardless of whether $Ca^{2+}$ was added to the *cis* or *trans* side (Figure 3A). However, typical step-like currents were observed in the $Na^+/Mg^{2+}$ solutions (Figure 3C). The current-voltage relationship plots indicate that the addition of 0.1:10 mM (*cis*:*trans*) $Mg^{2+}$ shifted the reversal potential of −63.7 mV for the asymmetric 15:150 mM (*cis*:*trans*) $Na^+$ solutions to −35.1 mV (Figure 3D), indicating that $MLKL^{E/D}$ channel is more permeable to $Mg^{2+}$ than to $Na^+$ ($P_{Mg}/P_{Na}$ = 2.8). A kinetics analysis revealed slightly different properties of the $Mg^{2+}$ currents in the $Na^+$and $Na^+/K^+$ solutions (Figure 3E). To further confirm that $Mg^{2+}$ could pass through $MLKL^{E/D}$ channels, pure $Mg^{2+}$ currents were isolated. The frequent and continuous outward $Na^+$ currents in the asymmetric 15:150 mM (*cis*:*trans*) $Na^+$ solutions indicated that the $MLKL^{E/D}$ channels were incorporated into the membrane. The membrane potential was then changed to the $Na^+$ equilibrium potential, −65 mV, to eliminate the $Na^+$ currents. Intriguingly, inward step-like signals appeared when 20 mM (final concentration) $Mg^{2+}$ was added to the *cis* side (Figure 3F, the upper trace). $Mg^{2+}$ currents were also observed in the $Na^+/K^+$ mixture solutions under identical condition (Figure 3F, the lower trace). A similar strategy was used to further examine the $Ca^{2+}$ permeability of the $MLKL^{E/D}$ channels. However, under identical condition, addition of 10 or 20 mM $Ca^{2+}$ did not induce inward currents, which supports a lack of $Ca^{2+}$ permeability (Figure 3B). Collectively,

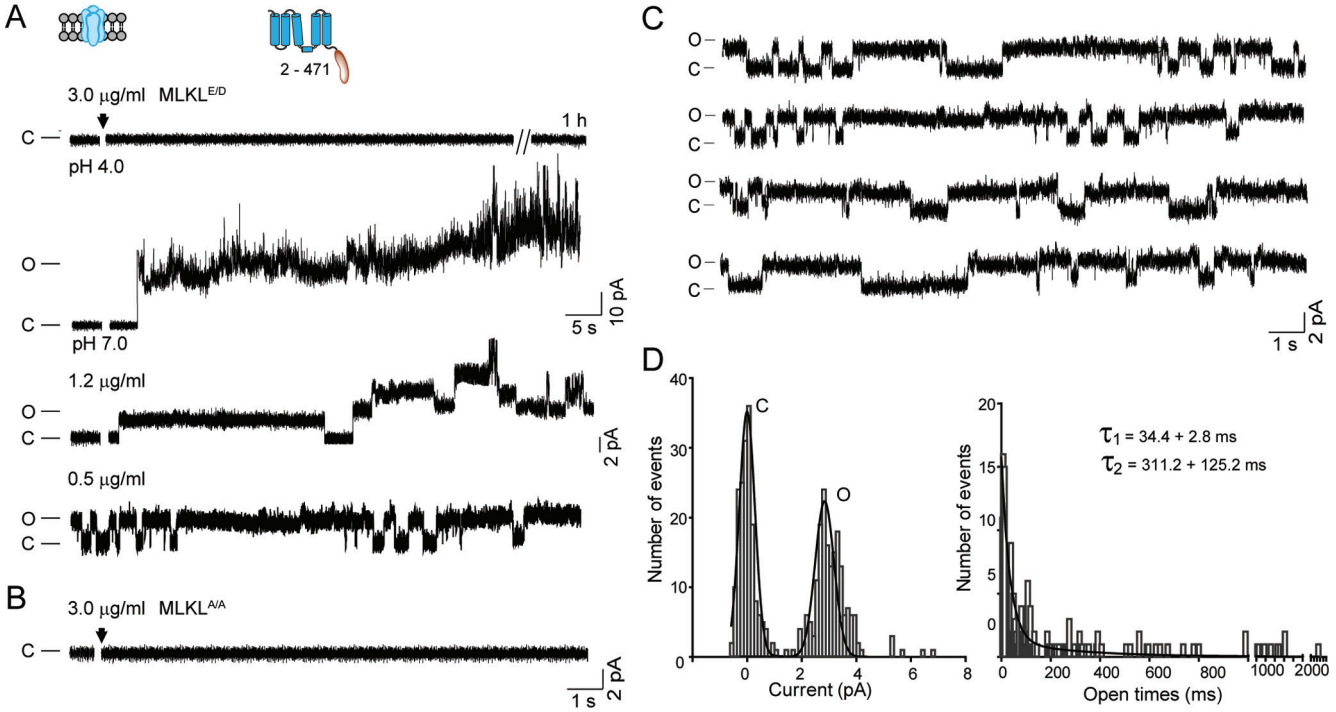


**Figure 1** MLKL mediates typical single-channel currents in planar lipid bilayer. **(A)** MLKL$^{E/D}$ (3.0 μg/ml) did not induce current-like signals for 1 h in low pH solutions (pH = 4.0) (upper panel). In neutral solutions (pH = 7.0), 3.0 μg/ml MLKL$^{E/D}$ induced large currents while 1.2 μg/ml MLKL$^{E/D}$ induced multi-conductance step-like signals (middle panel) . A reduced amount of MLKL$^{E/D}$ (0.5 μg/ml) induced typical single-channel currents (lower panel). Protein was added to the *cis* side of the symmetric 50 mM NaCl solutions, and the membrane potential was clamped at +50 mV (*trans* side). The *cis* side indicates the side the protein was added and the membrane potential represents the voltage potential at the *trans* side. pH was buffered to 7 for all solutions used in this study except otherwise stated. Inset: the schematic representation of bilayer lipid recording (left) and the purified MLKL (right). **(B)** MLKL$^{A/A}$ (3.0 μg/ml) did not induce step-like current signals. **(C)** A 70-second continuous recording of single-channel currents. **(D)** Left panel: all-points amplitude histogram generated from the continuous single-channel recording of **C**. The two peaks represent the current levels of the closed (C, left) and open (O, right) channel. The line represents a Gaussian fit to the binned data (bin width = 0.125 pA). Right panel: open-time histograms generated from more than 900 events. Lines are exponential fits to the binned data (bin width = 0.75 ms) from each data set ($n$ > 3).

these results demonstrate that the MLKL channels are preferentially permeable to $Mg^{2+}$ in the presence of $Na^+$ and $K^+$ ($P_{Mg} > P_{Na} \approx P_K >> P_{Ca}$ and $P_{Cl}$).

*N-terminal region is sufficient to form channels*

The N-terminal domain containing the HBD can trigger necroptosis or liposome leakage, whereas the C-terminal kinase-like domain lacks this capability and exerts inhibitory effects on MLKL-mediated membrane permeation [13, 20, 23, 24]. Whether the purified C-terminal kinase-like domain (MLKL$^{179-471}$) can mediate currents was examined first. Consistent with the inability to induce membrane permeation, the addition of MLKL$^{179-471}$ did not induce step-like signals (Figure 4A). Next, the N-terminal domain MLKL$^{2-178}$ was examined. We found that MLKL$^{2-178}$ could induce typical step-like signals in asymmetric 15:150 mM (*cis*:*trans*) NaCl solutions as the MLKL$^{E/D}$ (Figure 4B). Similarly to MLKL$^{E/D}$, MLKL$^{2-178}$ is $Na^+$, $K^+$ and $Mg^{2+}$ permeable but lacks $Ca^{2+}$ permeability (Supplementary information, Figure S2). Although MLKL$^{2-178}$ suffices to mediate step-like signals, one may argue that bilayer artifacts, such as collision of the protein with the membrane, may cause artificial signals. Two Flag-tagged proteins, MLKL$^{2-178}$-N-Flag and MLKL$^{2-178}$-C-Flag, with the Flag-tag fused to the N terminus or C terminus of MLKL$^{2-178}$, respectively, were constructed. Interestingly, only MLKL$^{2-178}$-C-Flag induced step-like signals, whereas MLKL$^{2-178}$-N-Flag did not induce detectable signals. Consistent with our results, the expression of N-terminal Flag-tagged full-length MLKL cannot induce necroptosis [23, 24]. Collectively, these results argue against the possibility that bilayer artifacts account for the recorded signals and indicate the essential role of the MLKL N-terminal region in channel formation.

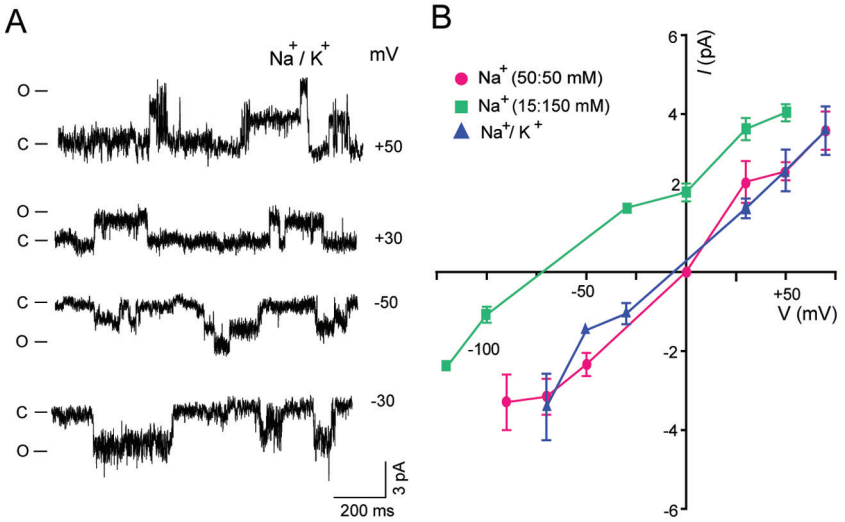


**Figure 2** Cation selectivity of MLKL channels. **(A)** Representative traces of $MLKL^{E/D}$ channels in $Na^+/K^+$ mixture solutions under indicated membrane potentials. **(B)** Current-voltage (*I-V*) plots demonstrating cation selectivity. The asymmetric (green squares) 15:150 mM (*cis*:*trans*) $Na^+$ solutions did not affect the linear *I-V* relationship but left-shifted the reversal potential to −63.7 mV. With the addition of 150:15mM (*cis*:*trans*) $K^+$ solutions to the $Na^+$ gradient, the reversal potential shifted to −6.0 mV from −63.7 mV, indicating that the $MLKL^{E/D}$ channels cannot distinguish $Na^+$ and $K^+$. The single-channel conductance in the symmetric $Na^+$ (magenta circles), the asymmetric $Na^+$ (green squares) and the $Na^+/K^+$ mixture (blue triangles) solutions was 45.9 ± 2.7, 36.7 ± 3.6, and 47.0 ± 8.7 pS, respectively ($n > 4$ for each group).

To further explore the minimum region that mediates the conductance, three truncations, $MLKL^{21-178}$, $MLKL^{2-154}$ and $MLKL^{2-125}$, were constructed based on the 3-D structure of human MLKL (PDB accession code 2MSV; Figure 4C). $MLKL^{21-178}$ lacks helix H1; $MLKL^{2-154}$ contains helices H1 to H6, and $MLKL^{2-125}$ does not have helix H6. $MLKL^{21-178}$ did not induce membrane permeability in a lipid bilayer, suggesting that helix H1 is critical for the channel function. Both $MLKL^{2-125}$and $MLKL^{2-154}$ also failed to induce typical ion channel signals. The truncation $MLKL^{2-125}$ initially induced an ~20 pA constitutive conductance. Shortly after, a huge conductance larger than 100 pA was observed, and the base line was not restored. Although the mechanism underlying the huge conductance of $MLKL^{2-125}$ in the late stage remains to be determined, the capability of $MLKL^{2-125}$ to permeabilize the membrane is consistent with the reports that the HBD (1-125) is sufficient to induce liposome leakage and cell death [21, 25]. These results support that the HBD is the core element for the MLKL-mediated permeability. Different from $MLKL^{2-125}$, $MLKL^{2-154}$ induced only unstable inward deflections with no step-like signals, suggesting both helix H6 and the following segment (residues 155-178) are essential for channel function. Consistent with the lack of channel activity of $MLKL^{2-154}$, it has been demonstrated that overexpression of the first 154 amino acids cannot induce cell death in HEK293 cells [25]. The N-terminal structure of human MLKL does not include residues 155-178, but it is suggested that they may form a coiled-coil secondary structure. The structure of full-length mouse MLKL (PDB accession code 4BTF) reveals that the corresponding residues to human MLKL 155-178 contain a 10-residue α-helix (159-168 in mouse) that is close to the C-terminal kinase-like domain. Taken together, for the $MLKL^{2-178}$ channel, the HBD that contains helices H1 to H5 is responsible for the conductivity, while helix H6 and the following segment of the protein are essential to maintain the channel in a normal state.

*Helices H1, H2, H3, H5 and H6 are transmembrane segments*

The N-terminal region of human MLKL contains six helices, H1 to H6 (Supplementary information, Figure S3). A recent study on the architecture of the apoptotic Bak pore suggested that the Bak helices orient nearly parallel to the plane of the membrane and the HBD of MLKL has been proposed to behave like Bak in the membrane [26]. In an ion channel, the helices are usually perpendicular to the membrane and are across the membrane. A substituted cysteine accessibility mutagenesis (SCAM) strategy was used to determine the configuration of these six helices in membrane [27]. SCAM has been wildly used to investigate the accessibility of residues lining the ion-permeation pathway in ion channel

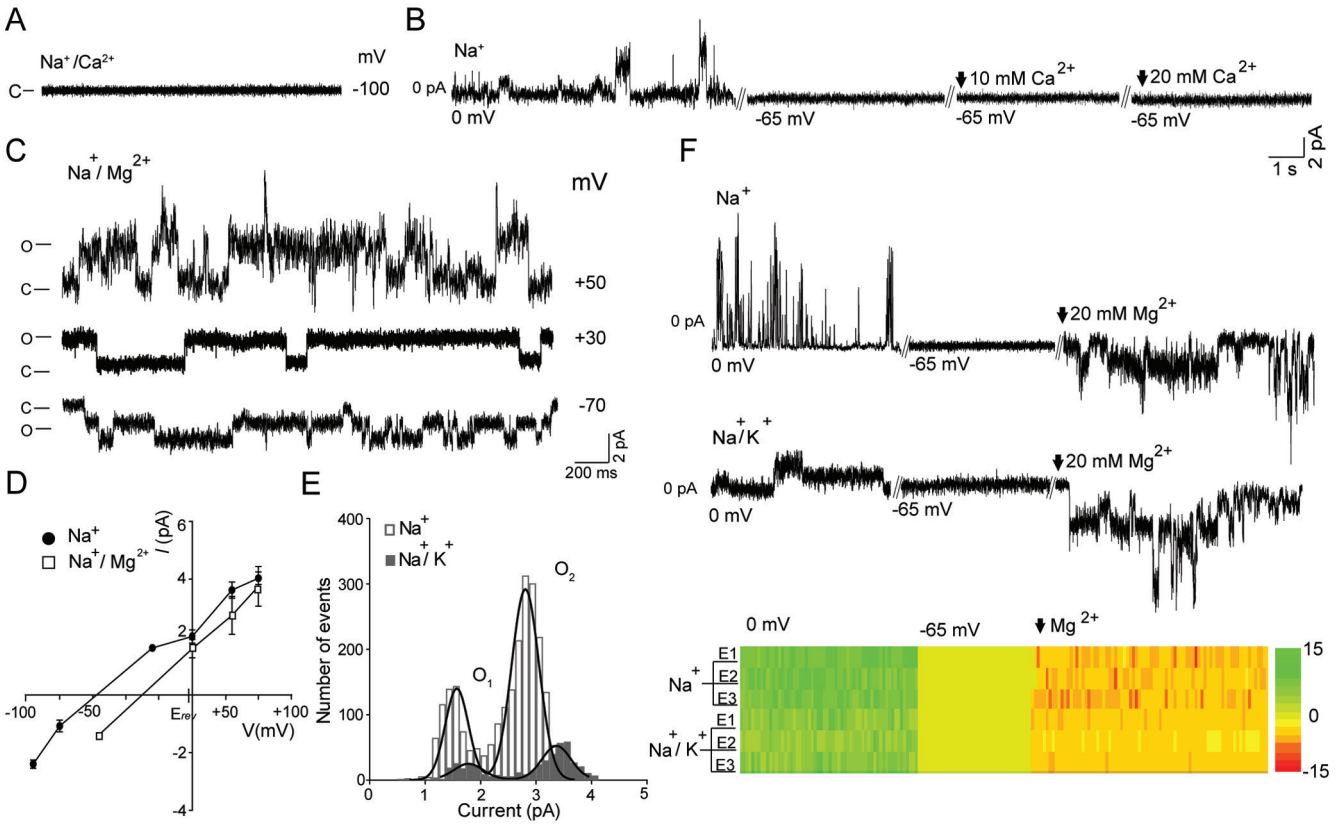


**Figure 3** MLKL forms $Mg^{2+}$-preferred channels. **(A)** $MLKL^{E/D}$ did not induce currents in the presence of $Na^+/Ca^{2+}$ mixture solutions. The *cis* side solution contained 15 mM $Na^+$ and 10 mM $Ca^{2+}$. The *trans* side solution contained 150 mM $Na^+$ and 0.1 mM $Ca^{2+}$. **(B)** Representative step-like currents in the asymmetric 15:150 mM (*cis*:*trans*) $Na^+$ solutions indicate the formation of $MLKL^{E/D}$ channels in the lipid membrane. The holding potential was next changed to −65 mV, the $Na^+$ equilibrium potential, to eliminate the $Na^+$ signals. $Ca^{2+}$ was subsequently added to the *cis* side to a final concentration of first, 10 mM, and then, 20 mM. **(C)** Representative traces of $MLKL^{E/D}$ in the $Na^+/Mg^{2+}$mixture solutions under the indicated holding potentials. The *cis* side solution contained 15 mM $Na^+$ and 10 mM $Mg^{2+}$. The *trans* side solution contained 150 mM $Na^+$ and 0.1 mM $Mg^{2+}$. **(D)** Current-voltage plots of $MLKL^{E/D}$ channels in the indicated solutions. $E_{rev}$ indicates the reversal potential of the pre-mixed $Na^+/Mg^{2+}$ solutions given that the permeability of $Mg^{2+}$ and $Na^+$ are equal. **(E)** All-points amplitude histogram of the $Mg^{2+}$ currents generated from the recordings presented in **B**. 'O1' and 'O2' indicate two open states of MLKL channels in indicated solutions. **(F)** $Mg^{2+}$ currents recorded in the $Na^+$ or $Na^+/K^+$ solutions. The heat map shows the transition of the currents in three individual experiments in $Na^+$ or $Na^+/K^+$ solutions. E1, E2 and E3 indicate three independent experiments.

proteins [28, 29]. MTSET (2-(trimethyl ammonium) ethyl methane thiosulfonate, bromide) is a membrane impermeant cysteine modification reagent. In principle, the cysteines, regardless of whether they are substituted or endogenous, would increase in bulk and positive charge after MTSET modification, which may consequently affect the channel function, if they are exposed to the hydrophilic environment [30]. In contrast to the cell or liposome system, the planar bilayer lipid membrane system used in this study allows the application of MTSET from either the *cis* or *trans* side (Figure 5A). The effects of MTSET on MLKL channels were opposite when it was applied on different sides (Figure 5B). The $MLKL^{2-178}$-mediated currents were inhibited by *trans* side MTSET. In contrast, this inhibition was not observed in the presence of *cis* side MTSET. There are four endogenous cysteines, C18 in helix H1, C24 and C28 in helix H2 and C86 in helix H4, in $MLKL^{2-178}$. These four cysteines were individually mutated to alanine (A), and the mutant C86A was no longer sensitive to MTEST (Figure 5C). The mutant C24A did not induce detectable currents (Supplementary information, Figure 3S), while mutants C18A and C28A exhibited similar sensitivity to MTSET compared with the wild-type channels, suggesting that these residues are not accessible or these positions are not sensitive to MTSET (Figure 5C). The residue C86 on which that MTSET acts is in the middle of the 9-residue helix H4. However, transmembrane helices are usually

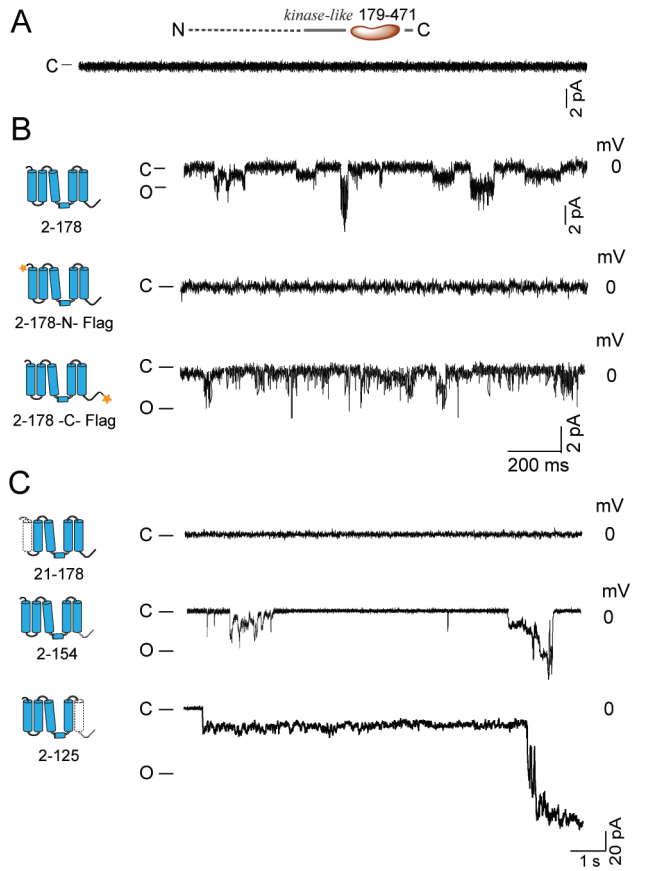


**Figure 4** MLKL N-terminal domain suffices to form channels. **(A)** C-terminal kinase-like domain (MLKL$^{179-471}$) did not induce step-like currents. **(B)** N-terminal domain (MLKL$^{2-178}$) sufficed to mediate step-like currents. **(C)** Representative traces induced by indicated truncations of the N-terminal domain. The truncated parts are indicated using dotted lines. All recordings were performed in asymmetric 15:150 mM (*cis*:*trans*) $Na^+$ solutions ($n$ > 4 for each group).

approximately 20 amino acids in length. In addition, the solution structure suggests that helix H4 interacts with the intracellular kinase-like domain [21]. Therefore, we conclude that helix H4 is located in the cytoplasm.

Based on the localization of H4, the helices H3 and H5 were then investigated. Residues D47 and S55 are in the H2-H3 loop, while Q120 is in the H5-H6 loop. *Cis* side MTSET could inhibit the mutant D47C, S55C or Q120C, suggesting that the helices H3 and H5 are transmembrane segments (Figure 5A and 5C). Since the endogenous cysteines, C18, C24 and C28, in the H1-H2 loop are not responsible for the inhibition by *trans* side MTSET, a new cysteine mutation Y23C was introduced into the C86A mutant. The mutant Y23C/C86A restored the sensitivity of C86A to MTSET on the *trans* side, revealing that helix H2 is a transmembrane segment (Figure 5C). Next, the L4 in the helix H1 N terminus was replaced by a cysteine. The mutant L4C could be inhibited by *cis* side MTSET, suggesting that helix H1 is also a transmembrane segment (Figure 5C). The H5-H6 loop is located on the opposite side of helix H4, while the kinase-like domain is in the cytoplasm. This finding suggests that the region comprised of helix H6 and the following segment, which connects to the kinase-like domain, contains a transmembrane segment. The double mutation C86A/D154C restored the sensitivity of C86A to MTSET on the *trans* side, indicating that helix H6 spans the membrane (Figure 5C). Mutants insensitive to MTSET modification can be found in Supplementary information, Figure S4. The channel activity of MLKL$^{2-178}$ mutants is correlated with their capability to induce cell death. In the *Mlkl* knockout Hela cells, overexpression of wild-type MLKL$^{2-178}$ or mutants that exhibit channel activity in the lipid bilayer membrane induced comparable cell death, whereas the mutants that lack channel activity, such as K22A, K22A/R30A, L45A and L45C, did not cause cell death (Supplementary information, Figure S5). Noticeably, it has been demonstrated previously that the K22A/R30A mutant cannot form oligomers and induce cell death [24]. Collectively, our data show that each MLKL monomer contains five transmembrane helices: H1, H2, H3 and H5 of the HBD and helix H6. Based on the MLKL truncation data (Figure 4), we suggest the four transmembrane segments of the HBD make up the core of the MLKL channel and the fifth transmembrane segment also plays an important role in channel function.

### *MLKL channel activity confers cell death*

We have shown that MLKL forms cation channels. To investigate the contribution of the channel activity to MLKL-induced cell death, wild-type MLKL-mCherry was ectopically coexpressed with RIP3-YFP in HEK293 cells. The cells exhibiting red fluorescence signals were examined using the whole-cell patch clamp technique 16-20 h after transfection. We found that depolarization stimulations induced significant spontaneous outward currents in cells co-expressing MLKL/RIP3 (Figure 6A). The average density of the outward currents at +80 mV was approximately 71.1 ± 11.2 pA/pF ($n$ = 17), which was much larger than the currents recorded in the control groups, including MLKL alone, RIP3 alone and vector alone (Figure 6A and 6B). Notably, the currents from the MLKL/RIP3 cells were outward rectified, with a reversal potential of 8.8 mV, whereas the current-voltage plots of the control groups were linear, with a reversal potential of 0 mV. In addition, the recorded currents were not sensitive to inhibitors of sodium, potassium, calcium and TRPM7 channels (Supplementary information, Figure

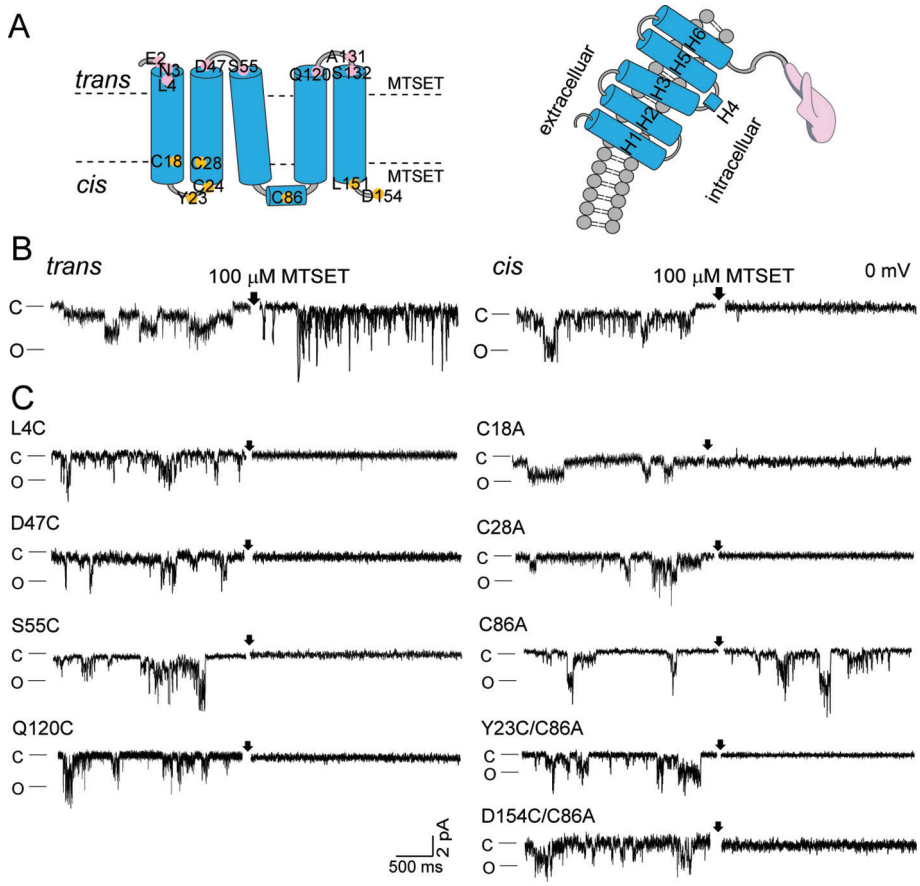


**Figure 5** Identification of transmembrane segments. **(A)** Left: schematic representation of the residues examined and the corresponding six α-helices revealed by the solution MLKL structure. The dotted lines indicate the hypothetical lipid bilayer. MTSET is applied from either the *cis* or *trans* side. Mutations for MTSET test from *cis* (small lilac balls) or *trans* (small yellow balls) side are indicated. Right: topology of one subunit of MLKL channel. The dotted lines and gray circles represent the cellular membrane. The C-terminal kinase-like domain is colored in pink. **(B)** Responses of wild-type MLKL$^{2\text{-}178}$ to MTSET. The black arrow indicates the application of MTSET. **(C)** Responses of indicated mutants to MTSET. The currents were recorded in asymmetric 15:150 mM (*cis*:*trans*) $Na^+$ solutions ($n$ > 4 for each group). MTSET (100 μM) was applied either in *cis* or *trans* side as described in Materials and Methods.

S6). In bilayer lipid membrane, the phosphomimetic mutant MLKL$^{E/D}$ formed channels, whereas the mutation MLKL$^{A/A}$ did not mediate currents. Consistently, enhanced whole-cell outward currents were observed for the phosphomimetic mutant MLKL$^{E/D}$, whereas expression of the MLKL$^{A/A}$ mutant did not induce significant currents (Figure 6A-6C). However, the MLKL$^{E/D}$ currents were smaller than the MLKL/RIP3 currents. The expression of MLKL/RIP3 induced time-dependent cell death and depolarization of the membrane potential (Figure 6D). In comparison to MLKL/RIP3, the expression of MLKL$^{E/D}$ induced moderate cell death and depolarization of membrane potential, whereas MLKL$^{A/A}$ did not cause these effects. The whole-cell current density, depolarization of the membrane potential and cell death induced by MLKL/RIP3, MLKL$^{E/D}$ and MLKL$^{A/A}$ were positively correlated with each other (Figure 6E). In addition, mutations such as L45A and L45C, which block channel activity, were found to be able to rescue the MLKL-induced cell death (Supplementary information, Figure S5). These results indicate that the channel activity of MLKL confers cell death.

## Discussion

MLKL is a pseudokinase and cannot transduce necrosis signals through phosphorylation of downstream effectors. Previous studies reported that $Na^+$ or $Ca^{2+}$ influx potentially contributes to cell necrosis after MLKL oligomerization and translocation to the membrane, suggesting that certain types of channels activated downstream of MLKL might be responsible for the ion influxes [22,

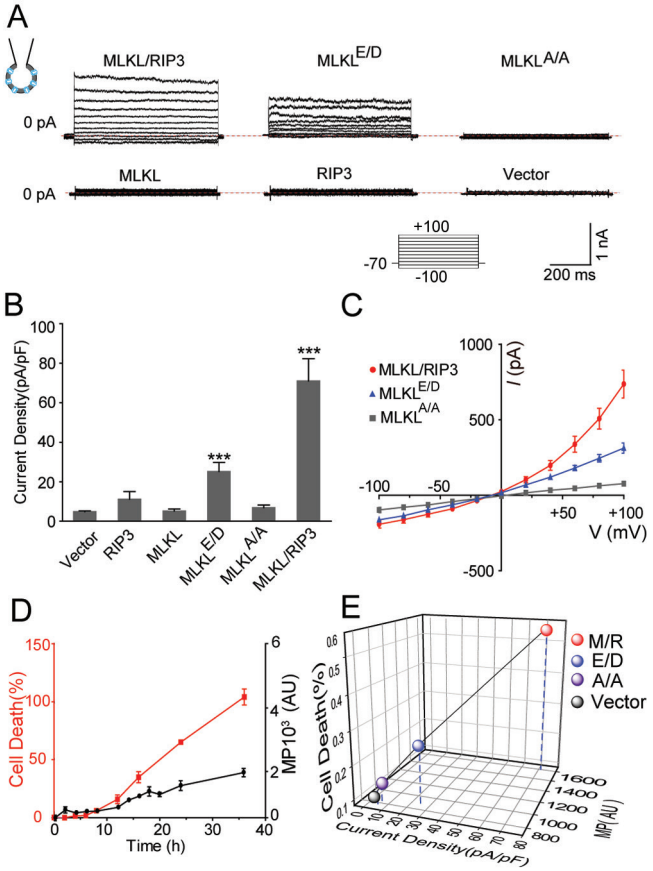


**Figure 6** The correlation between channel activity and MLKL-induced cell death. **(A)** Representative whole-cell currents induced by the expression of indicated constructs. The inset shows the protocol applied to elicit the currents. The currents elicited by +60 mV are used to calculate the current density. Inset: schematic representation of the whole-cell recording. **(B)** Current density of the currents induced by the constructs shown in **A** ($n$ > 8). **(C)** Current-voltage ($I$-$V$) plots. For clarity, only the $I$-$V$ plots of MLKL/RIP3, MLKL$^{E/D}$ and MLKL$^{A/A}$ are shown ($n$ > 8). **(D)** Time-dependent cell death (red line) and membrane potential depolarization (black line) induced by coexpressing MLKL/RIP3. Time (h) indicates the time after transfection. **(E)** The correlation between the current density, depolarization of the membrane potential and cell death induced by the indicated constructs. The parameters were measured 16-20 h after transfection. 'M/R' indicates MLKL/RIP3; 'E/D' indicates MLKL$^{E/D}$; 'A/A' indicates MLKL$^{A/A}$.

23]. In this study, we show that MLKL itself forms a cation channel with following properties. First, in a bilayer lipid membrane, MLKL mediates typical single-channel currents. Second, the conductance mediated by MLKL exhibits ionic selectivity, which is a key property of ion channels. Third, five transmembrane segments and their orientations deduced in our study, together with the unique ionic selectivity, define MLKL as a new type of ion channel. The channel activity of MLKL is correlated with MLKL-induced cell death (Figure 6). Consistent with its $Na^+$ permeability, an increased intracellular $Na^+$ concentration has been observed during necroptosis, and $Na^+$ depletion in the culture medium delays necroptosis in L929 cells [23]. The identification of MLKL as an ion channel confirms that the disturbance of intracellular ion homeostasis by MLKL is a critical step of necroptosis [22, 23].

The structures of both mouse MLKL and human MLKL contain a HBD in the N terminus [13, 19]. Consistent with its essential role in necroptosis or liposome leakage, our study shows the HBD is also essential for the channel formation. In addition to full-length MLKL with phosphomimetic mutations, MLKL$^{2\text{-}178}$, which contains the HBD and helix H6, mediates typical step-like currents. In contrast, MLKL$^{2\text{-}154}$ cannot induce step-like currents. Its opening is clearly unstable and larger than the one induced by MLKL$^{2\text{-}178}$. The shortest fragment, MLKL$^{2\text{-}125}$, which contains only the HBD, induces an even larger conductance and eventually causes damages in the membrane. A previous study of liposome leakage induced by truncated MLKL revealed that HBD alone has a higher permeation efficiency than MLKL$^{2\text{-}154}$, which contains the HBD and helix H6 [13]. These results suggest that MLKL HBD, helix H6 and the following segment (154-178) are necessary and sufficient to form a typical cation channel, although the HBD alone can mediate membrane permeation. The enlarged conductance induced by the two shorter mutants, MLKL$^{2\text{-}154}$ and MLKL$^{2\text{-}125}$, reconciles apparently conflicting permeability of MLKL in the planer bilayer lipid membrane, liposomes and necrotic cells. The leakage of 10-kDa dextran (approximately 46 Å in diameter) from the liposome suggests the formation of huge pores in the liposome by MLKL [13]. In necrotic cells, $Na^+$ influx occurs at the beginning of MLKL oligomerization, while propidium iodide (PI) uptake, an indication of irreversible plasma membrane damage, occurs at a late stage of necrosis [23]. Consistently, during necroptosis, the permeation of the membrane of cellular organelles, such as lysosomal membrane permeabilization and mitochondrial hyperpolarization, occurs before the PI uptake [31]. The damage to cellular organelles may be caused by MLKL directly or by a disturbance of the intracellular ion equilibrium by MLKL channels. Accordingly, one possibility is that MLKL may form selective channels at an early stage of necroptosis and then self-assemble to larger pores to cause membrane lysis. Whether and how MLKL transforms from selective channels to large unselective pores remains to be investigated.

Determining the configuration of MLKL in the mem-

brane is crucial for understanding the regulation of MLKL channels. SCAM is usually used to investigate positions of the residues lining the permeation pathway in an ion channel. In this study, SCAM was used to determine the potential membrane spanning segments. Five transmembrane segments, helices H1, H2, H3, H5, and H6, were identified. Helix H1 is the first transmembrane segment with its N terminus facing the extracellular side. The responses of mutants D47C and S55C to MTSET define a H2-H3 loop facing the extracellular side. Inhibition of the mutant Q120C by MTSET defines the transmembrane helix H5. Helix H4 is located in the cytoplasm. Helix linkers that couple the pore domain and the peripheral domains are often observed in six-transmembrane ion channels, such as voltage-gated potassium (Kv) channels and TRP channels. Although helix H4 has been identified to be the target of necrosulfonamide, which can block MLKL oligomerization [32], whether it can function like the linkers in Kv or TRP channels is currently unknown. The lack of response of some mutants such as E2C, N3C, A131C, S132C and M151C (Supplementary information, Figure S4) could be due to multiple reasons. First, these residues may be buried in the lipid bilayer. Second, MTSET modification does occur at these residues but it has no effect on the channel conductivity. Third, other factors, such as the nearby residues in 3-D space, may hinder the access of MTSET to these residues. Taken together, we demonstrate that MLKL channels consist of at least five transmembrane helical segments per monomer, with the N terminus facing the extracellular side and the C terminus facing the intracellular side (Figure 5A).

$Mg^{2+}$ regulates myriad cellular functions and serves as an intracellular second messenger [33-37]. In the cytosol or organelles, the total $Mg^{2+}$ concentration ranges between 14 and 20 mM, whereas only 1%-5% $Mg^{2+}$ is in the free state due to buffering by polyphosphates, free nucleotides and nucleic acids [33, 38]. The concentration of intracellular free $Mg^{2+}$ is about 100-fold below its electrochemical equilibrium potential, which theoretically allows $Mg^{2+}$ influxes [37, 39, 40]. However, the molecular mechanism of $Mg^{2+}$ movement across the membrane has not been well elucidated. A less than ideal $Mg^{2+}$ fluorescence indicator, mag-fluo-4, has been used to monitor the MLKL-dependent $Mg^{2+}$ influx. In the HEK 293 cells expressing MLKL/RIP3, extracellular application of $Mg^{2+}$ induced a significant increase in fluorescence intensity (Supplementary information, Figure S7). Consistently, elevated extracellularly $Mg^{2+}$ hyperpolarized the membrane potential of the HEK 293 cells expressing MLKL/RIP3 (Supplementary information, Figure S8). TRPM6 and TRPM7 are two identified ion channels expressed in the plasma membrane with permeability to $Mg^{2+}$. However, they are also permeable to $Ca^{2+}$ [41]. MLKL channels are preferentially permeable to $Mg^{2+}$ but not to $Ca^{2+}$, which distinguishes them from these two channels. As a six-transmembrane spanning domain protein, the $Mg^{2+}$-permeable TRPM7 has been reported to be a downstream target of MLKL [22]. In addition to the lack of permeability to $Ca^{2+}$ (Figure 2C), MLKL channels are also insensitive to NS8593, an inhibitor of TRPM7 channels (Supplementary information, Figure S6). However, a rise in cytosolic $Ca^{2+}$ caused by an extracellular $Ca^{2+}$ influx has been observed in necroptosis [22]. Therefore, the possibility that $Ca^{2+}$-permeable channels are involved downstream of MLKL cannot be excluded. The influx of $Mg^{2+}$ into organelles, such as mitochondria, has been proposed via a uniporter or by an 'unspecific leak' until the identification of Mrs2p. Mrs2p is a distant relative of the bacterial CorA and yeast Alr1p $Mg^{2+}$ transport protein families and appears to be the essential constituent of the mitochondrial $Mg^{2+}$ influx system, presumably forming a homo-oligomeric $Mg^{2+}$ channel [42, 43]. Both Mrs2p and CorA have been demonstrated to be a funnel-shaped homopentamer with two transmembrane segments per monomer [42, 44, 45]. In addition, some $Mg^{2+}$ transporters, such as MgtE and its distant homologue SLC41A1, have been cloned and characterized [46, 47]. However, the crystal structure reveals MgtE to be a homodimer, whereas MLKL forms either a trimer or a tetramer [22, 23, 48]. In particular, MgtE is not permeable to monovalent $Na^{+}$ and $K^{+}$ [48]. Noticeably, among these $Mg^{2+}$-permeable channels or transporters, only TRPM6 and TRPM7 channels have been found to mediate macroscopic whole-cell currents as MLKL channels do [49, 50]. Taken together, the $Mg^{2+}$-preferred permeability and five transmembrane segment topology establish MLKL as a novel class of cation channel. Further investigation on how the $Mg^{2+}$ permeability of MLKL channels contributes to necroptosis execution would promote the understanding of this form of programmed cell death.

## Materials and Methods

*Plasmids and mutagenesis*

The MLKL and RIP3 plasmids used in whole-cell recording and cell survival assay were provided by Dr Z Liu (NCI, NIH) and were cloned into pLenti-CMV-mCherry-3FLAG and pEYFP-N1 vector, respectively, to produce pEGFP-N1-MLKL and pYFP-N1-RIP3. The TRPM7 plasmid was a gift from Dr D Clapham (Harvard Medical School). Point mutations were generated using sited-directed mutagenesis and confirmed by sequencing.

*Protein purification*

Full-length human MLKL and MLKL kinase-like domain were expressed in SF21 cells according to the manufacturer's protocol (Life Technology). Human $MLKL^{2-178}$, $MLKL^{2-154}$, and $MLKL^{2-125}$

were expressed in *E.coli* BL21/DE3. Recombinant proteins were purified using glutathione-Sepharose affinity chromatography (Yishen), and the GST-tag is removed by precision protease (NEB).

*Planer bilayer lipid membrane recording*

The currents of purified MLKL proteins were recorded in a voltage-clamp mode using a Warner BC-535 bilayer clamp amplifier (Warner Instruments) filtered at 1-2 kHz. The currents were digitized using pCLAMP 10.2 software (Molecular Devices). Data are presented as the mean ± SEM. Lipid bilayers were formed using phosphatidylcholine (PC):Phosphatidylserine (PS) = 3:2 (Avanti Polar Lipids). The single-channel conductance and open time were determined by fitting to Gaussian functions or to single or bi-exponential equations. Opening times < 0.5-1.5 ms were ignored. The equilibrium potential was calculated using the Nernst equation, and the ion selectivity was calculated using the Goldman-Hodgkin-Katz flux equation.

a. Monovalent ion: $E_{rev} = RT/zF \times \ln(P_{K^+}[K^+]_o/P_{Na^+}[Na^+]_i)$

b. Divalent ion: $E_{rev} = RT/zF \times \ln(\sqrt{((4P_{Ca^{2+}}[Ca^{2+}]_o/P_{Na^+}[Na^+]_i) + 1/4) - 1/2)}$

*Substituted cysteine accessibility mutagenesis (SCAM)*

The stock solution of MTSET (Biotium) was 20 mM in water and was stored at −20 °C. MTSET at a final concentration of 100 μM was applied either in *cis* or *trans* side using pipette manually. The constructs with currents that were not inhibited 5 min after MTSET application were defined as in-sensitive; the constructs whose currents were inhibited and were not restored in 10 min were defined as sensitive.

*Cell culture and transient transfection*

Human embryonic kidney 293 (HEK293) cells were grown in DMEM with 10% fetal bovine serum, 2 mM L-glutamine and 100 units/ml penicillin/streptomycin. To express MLKL channels or other proteins, HEK293 cells were split at 24 h before transfection, plated in 60-mm dishes, and transfected with Lipofectamine 2000™ reagent (Life Technology) according to the manufacturer's instruction. At 16 h after transfection, cells were replated onto coverslips coated with poly-L-lysine (Sigma-Aldrich) for recording.

*Whole-cell recording*

MLKL currents were recorded using an Axopatch 200B amplifier (Molecular Devices). $Mg^{2+}$-free intracellular and extracellular solutions were used unless otherwise stated. The series resistance was compensated by 60%-80%.

*Cell survival assay*

Cell viability was examined using the CellTiter-Glo Luminescent Cell Viability Assay kit (Promega) according to the manufacturer's instruction. Luminescence was recorded with Biotek Synergy2 Luminescent plate reader (Biotek Winooski).

*$Mg^{2+}$ influx assay*

$Mg^{2+}$ influx was examined using the fluorescence indicator mag-fluo-4 (Life Technology) according to the manufacturer's instruction. Mag-fluo-4 was excited at 340 and 380 nm with a rapid switching monochromator (TILL Photonics), and the mean fluorescence intensity ratios ($F_{340}/F_{380}$) showed the changes of intracellular free $Mg^{2+}$ in real time.

*Membrane potential measurement*

Membrane potential of HEK293 was measured using a membrane potential assay kit (Molecular Devices) following the manufacturer's protocol with some modification. Briefly, cell plates were loaded with assay buffer containing 1× membrane-potential dye. After a 40-min incubation at room temperature in darkness, the plates were placed on the platform of FDSS (Hamamatsu), and the fluorescence was read with excitation/emission at 488/540 nm. After 10 seconds of recording, 50 μl/well of standard external solution buffer was added. The plates were read every second for 300 s.

## Acknowledgments

This work was supported by the State Key Program of Basic Research of China (2013CB910604), the National Natural Science Foundation of China (61327014, 61175103, 61433017 and 31571427) and the External Cooperation Program of BIC, Chinese Academy of Sciences (1536631KYSB20130003).

*Author Contributions*

BX and XC performed electrophysiological experiments. BX, HW, SF, HH, and PC performed cell biology experiments. ZG, HW, and BX designed the experiments, and wrote the manuscript.

*Competing Financial Interests*

The authors declare no competing financial interests.

## References

1 Pasparakis M, Vandenabeele P. Necroptosis and its role in inflammation. *Nature* 2015; **517**:311-320.
2 Sun L, Wang X. A new kind of cell suicide: mechanisms and functions of programmed necrosis. *Trends Biochem Sci* 2014; **39**:587-593.
3 Grooten J, Goossens V, Vanhaesebroeck, *et al*. Cell membrane permeabilization and cellular collapse, followed by loss of dehydrogenase activity: early events in tumour necrosis factor-induced cytotoxicity. *Cytokine* 1993; **5**:546-555.
4 Laster SM, Wood JG, Gooding LR. Tumor necrosis factor can induce both apoptic and necrotic forms of cell lysis. *J Immunol* 1988; **141**:2629-2634.
5 Vercammen D, Beyaert R, Denecker G, *et al.* Inhibition of caspases increases the sensitivity of L929 cells to necrosis mediated by tumor necrosis factor. *J Exp Med* 1998; **187**:1477-1485.
6 Feoktistova M, Leverkus M. Programmed necrosis and necroptosis signalling. *FEBS J* 2015; **282**:19-31.
7 Dunai ZA, Imre G, Barna G, *et al*. Staurosporine induces necroptotic cell death under caspase-compromised conditions in U937 cells. *PLoS One* 2012; **7**:e41945.
8 Kaiser WJ, Sridharan H, Huang C, *et al.* Toll-like receptor 3-mediated necrosis via TRIF, RIP3, and MLKL. *J Biol Chem* 2013; **288**:31268-31279.
9 Schworer SA, Smirnova, II, Kurbatova I, *et al.* Toll-like receptor-mediated down-regulation of the deubiquitinase cylindromatosis (CYLD) protects macrophages from necroptosis in wild-derived mice. *J Biol Chem* 2014; **289**:14422-14433.

10 Tenev T, Bianchi K, Darding M, *et al.* The Ripoptosome, a signaling platform that assembles in response to genotoxic stress and loss of IAPs. *Mol Cell* 2011; **43**:432-448.
11 Upton JW, Kaiser WJ, Mocarski ES. DAI/ZBP1/DLM-1 complexes with RIP3 to mediate virus-induced programmed necrosis that is targeted by murine cytomegalovirus vIRA. *Cell Host Microbe* 2012; **11**:290-297.
12 Han W, Li L, Qiu S, *et al.* Shikonin circumvents cancer drug resistance by induction of a necroptotic death. *Mol Cancer Ther* 2007; **6**:1641-1649.
13 Wang H, Sun L, Su L, *et al.* Mixed lineage kinase domain-like protein MLKL causes necrotic membrane disruption upon phosphorylation by RIP3. *Mol Cell* 2014; **54**:133-146.
14 Cho YS, Challa S, Moquin D, *et al.* Phosphorylation-driven assembly of the RIP1-RIP3 complex regulates programmed necrosis and virus-induced inflammation. *Cell* 2009; **137**:1112-1123.
15 Degterev A, Huang Z, Boyce M, *et al.* Chemical inhibitor of nonapoptotic cell death with therapeutic potential for ischemic brain injury. *Nat Chem Biol* 2005; **1**:112-119.
16 He S, Wang L, Miao L, *et al.* Receptor interacting protein kinase-3 determines cellular necrotic response to TNF-α. *Cell* 2009; **137**:1100-1111.
17 Li J, McQuade T, Siemer AB, *et al.* The RIP1/RIP3 necrosome forms a functional amyloid signaling complex required for programmed necrosis. *Cell* 2012; **150**:339-350.
18 Zhang DW, Shao J, Lin J, *et al.* RIP3, an energy metabolism regulator that switches TNF-induced cell death from apoptosis to necrosis. *Science* 2009; **325**:332-336.
19 Murphy JM, Czabotar PE, Hildebrand JM, *et al.* The pseudokinase MLKL mediates necroptosis via a molecular switch mechanism. *Immunity* 2013; **39**:443-453.
20 Dondelinger Y, Declercq W, Montessuit S, *et al.* MLKL compromises plasma membrane integrity by binding to phosphatidylinositol phosphates. *Cell Rep* 2014; **7**:971-981.
21 Su L, Quade B, Wang H, *et al*. A plug release mechanism for membrane permeation by MLKL. *Structure* 2014; **22**:1489-1500.
22 Cai Z, Jitkaew S, Zhao J, *et al.* Plasma membrane translocation of trimerized MLKL protein is required for TNF-induced necroptosis. *Nat Cell Biol* 2014; **16**:55-65.
23 Chen X, Li W, Ren J, *et al.* Translocation of mixed lineage kinase domain-like protein to plasma membrane leads to necrotic cell death. *Cell Res* 2014; **24**:105-121.
24 Hildebrand JM, Tanzer MC, Lucet IS, *et al.* Activation of the pseudokinase MLKL unleashes the four-helix bundle domain to induce membrane localization and necroptotic cell death. *Proc Natl Acad Sci USA* 2014; **111**:15072-15077.
25 Arnez KH, Kindlova M, Bokil NJ, *et al*. Analysis of the N-terminal region of human MLKL, as well as two distinct MLKL isoforms, reveals new insights into necroptotic cell death. *Biosci Rep* 2015; **36**:e00291.
26 Aluvila S, Mandal T, Hustedt E, *et al*. Organization of the mitochondrial apoptotic BAK pore: oligomerization of the BAK homodimers. *J Biol Chem* 2014; **289**:2537-2551.
27 Karlin A, Akabas MH. Substituted-cysteine accessibility method. *Methods Enzymol* 1998; **293**:123-145.
28 Fatehi M, Linsdell P. Novel residues lining the CFTR chloride channel pore identified by functional modification of introduced cysteines. *J Membr Biol* 2009; **228**:151-164.
29 Tombola F, Pathak MM, Gorostiza P, *et al*. The twisted ion-permeation pathway of a resting voltage-sensing domain. *Nature* 2007; **445**:546-549.
30 Tombola F, Pathak MM, Isacoff EY. How does voltage open an ion channel? *Annu Rev Cell Dev Biol* 2006; **22**:23-52.
31 Vanden Berghe T, Vanlangenakker N, Parthoens E, *et al*. Necroptosis, necrosis and secondary necrosis converge on similar cellular disintegration features. *Cell Death Differ* 2010; **17**:922-930.
32 Sun L, Wang H, Wang Z, *et al.* Mixed lineage kinase domain-like protein mediates necrosis signaling downstream of RIP3 kinase. *Cell* 2012; **148**:213-227.
33 Romani AM. Cellular magnesium homeostasis. *Arch Biochem Biophys* 2011; **512**:1-23.
34 Jung DW, Apel L, Brierley GP. Matrix free $Mg^{2+}$ changes with metabolic state in isolated heart mitochondria. *Biochemistry* 1990; **29**:4121-4128.
35 Rutter GA, Osbaldeston NJ, McCormack JG, *et al*. Measurement of matrix free $Mg^{2+}$ concentration in rat heart mitochondria by using entrapped fluorescent probes. *Biochem J* 1990; **271**:627-634.
36 Rodriguez-Zavala JS, Moreno-Sanchez R. Modulation of oxidative phosphorylation by $Mg^{2+}$ in rat heart mitochondria. *J Biol Chem* 1998; **273**:7850-7855.
37 Li FY, Chaigne-Delalande B, Kanellopoulou C, *et al.* Second messenger role for $Mg^{2+}$ revealed by human T-cell immunodeficiency. *Nature* 2011; **475**:471-476.
38 Grubbs RD. Intracellular magnesium and magnesium buffering. *Biometals* 2002; **15**:251-259.
39 Murphy E. Mysteries of magnesium homeostasis. *Circ Res* 2000; **86**:245-248.
40 Romani AM. Magnesium homeostasis in mammalian cells. *Front Biosci* 2007; **12**:308-331.
41 Li M, Jiang J, Yue L. Functional characterization of homo- and heteromeric channel kinases TRPM6 and TRPM7. *J Gen Physiol* 2006; **127**:525-537.
42 Kolisek M, Zsurka G, Samaj J, *et al*. Mrs2p is an essential component of the major electrophoretic $Mg^{2+}$ influx system in mitochondria. *EMBO J* 2003; **22**:1235-1244.
43 Schindl R, Weghuber J, Romanin C, *et al*. Mrs2p forms a high conductance $Mg^{2+}$ selective channel in mitochondria. *Biophys J* 2007; **93**:3872-3883.
44 Lunin VV, Dobrovetsky E, Khutoreskaya G, *et al.* Crystal structure of the CorA $Mg^{2+}$ transporter. *Nature* 2006; **440**:833-837.
45 Maguire ME. The structure of CorA: a $Mg^{2+}$-selective channel. *Curr Opin Struct Biol* 2006; **16**:432-438.
46 Wolf FI, Torsello A, Fasanella S, *et al*. Cell physiology of magnesium. *Mol Aspects Med* 2003; **24**:11-26.
47 Quamme GA. Molecular identification of ancient and modern mammalian magnesium transporters. *Am J Physiol Cell Physiol* 2009; **298**:C407-C429.
48 Takeda H, Hattori M, Nishizawa T, *et al.* Structural basis for ion selectivity revealed by high-resolution crystal structure of $Mg^{2+}$ channel MgtE. *Nat Commun* 2014; **5**:5374.
49 Li M, Du J, Jiang J, *et al.* Molecular determinants of $Mg^{2+}$ and $Ca^{2+}$ permeability and pH sensitivity in TRPM6 and TRPM7. *J Biol Chem* 2007; **282**:25817-25830.

50 de Baaij JH, Blanchard MG, Lavrijsen M, *et al*. P2X4 receptor regulation of transient receptor potential melastatin type 6 (TRPM6) $Mg^{2+}$ channels. *Pflugers Archiv* 2014; **466**:1941-1952.

(**Supplementary information** is linked to the online version of the paper on the *Cell Research* website.)